

Piezoelectric MEMS Energy Harvester from Airflow at Low Flow Velocities

Kensuke Kanda,* Takashi Aiba, and Kazusuke Maenaka

Graduate School of Engineering, University of Hyogo, 2167 Shosha, Himeji 671-2280, Japan

(Received February 16, 2022; accepted April 19, 2022)

Keywords: energy harvesting, MEMS, PZT, wind energy source, self-oscillation

Similarly to a harmonica reed, a piezoelectric MEMS cantilever is self-excited by an airflow. An airflow-induced self-excited vibration can be utilized as an energy source for energy-harvesting devices. In this study, with the aim of reducing the cut-in flow velocity, which is the lowest flow velocity required for resonant vibration, a thin MEMS structure with an intentionally warped shape was exploited in an energy harvester based on the principle of harmonica reeds. By compensating for the residual stresses of PZT and Pt electrode films, the cantilever warpage of the harvester structure can be controlled. The thin-film nature and the warped PZT/Si laminated MEMS structure enabled energy harvesting from an airflow at low flow velocities. Moreover, the cut-in flow velocity of the airflow-induced MEMS harvesting device was very low (1.2 m/s, one-tenth of that of a conventional device), and an output power of 3.84 μW was obtained at a flow velocity of 3.7 m/s.

1. Introduction

Our rapidly developing Internet of Things (IoT)-based society requires a large number of sensors. For IoT sensors, batteries cannot be adopted as power sources because of the economic and environmental costs of replacement and disposal. Hence, energy harvesting technology has recently attracted much attention, and many researchers have been devoted to this field during the last two decades. Energy can be harvested from various energy sources, such as sunlight, thermoelectricity, radio waves, wind, and mechanical vibration. Mechanical vibration is suitable for IoT sensors because of its high energy density and ubiquitous nature.^(1,2) To obtain electrical energy from mechanical vibration, energy conversion mechanisms are employed, such as piezoelectric, electromagnetic, and electrostatic mechanisms. A popular vibration harvesting strategy is to install a harvesting device on an external vibration source, where the device is resonantly vibrated to increase the vibration amplitude and obtain a large output power. However, this resonant-type harvester has a major drawback: its resonant frequency should equal the vibration frequency of the external vibration.⁽³⁾ In addition, whereas a large quality (Q) factor of vibration is preferred to obtain large output power, it leads to a narrow bandwidth. A nonlinear vibration and snap-through structure to widen the bandwidth, a mechanism for

*Corresponding author: e-mail: kanda@eng.u-hyogo.ac.jp
<https://doi.org/10.18494/SAM3867>

resonant frequency tuning, and a damped vibration mechanism based on shock inputs were previously investigated.^(4–7) Nevertheless, the widespread use of such vibration-type energy-harvesting devices is hindered by the small number of applications that can generate input vibrations with stable frequencies and sufficient amplitudes.

Self-excited vibration induced by an airflow is also a promising energy harvesting strategy. Mechanical resonant vibration can even be excited by a non-oscillatory airflow.⁽⁸⁾ There are two types of vibration energy harvesters based on self-excitation. First, similarly to in a harmonica reed, elastic beams placed on a resonant cavity are self-excited by the pressure fluctuation of an airflow.^(9–14) Second, vortex-induced vibration (VIV) is used as an excitation source.^(15,16) For the former case, air pressure in a cavity opens a bendable reed, and the fluctuation of the pressure induces self-excited vibration of the reed. For the latter case, vortices generated behind bluff bodies induce self-excited vibrations of the structure. For both cases, the body vibrates at its structural resonant frequency. The electrical energy is converted from mechanical vibration energy via energy conversion mechanisms such as piezoelectricity. A challenge in flow-induced energy harvesting is to reduce the cut-in flow velocity, which is the minimum, flow velocity at which self-excitation of the vibrator occurs. In this study, we focus on piezoelectric MEMS energy harvesters based on a free reed. Although the mechanism of the self-excited vibration of reeds is not completely clear, a mass-damper-spring ramped model has been proposed for the numerical calculation of free reeds.⁽¹⁷⁾ In general, harmonica reeds have a warped shape against the airflow, and this warpage strongly affects the dynamic behavior of the reeds. Most conventional harvesters based on harmonica reeds have a mechanism involving flow-induced self-excited oscillations of piezoelectric beams embedded in cavities and exploit bulk piezoelectric ceramics or polymers.^(9–11) An airflow-based energy harvester, which has a bulky rigid structure, requires a high flow velocity to bend the vibration structure. Although MEMS energy-harvesting devices have also been reported, it is difficult to obtain a large output power and a low cut-in flow velocity.^(12–14) To achieve a large output power and a low cut-in flow velocity, a piezoelectric MEMS energy-harvesting device having an intentionally warped shape and $\text{Pb}(\text{Zr,Ti})\text{O}_3$ (PZT) thin films with a thickness of 10 μm was microfabricated and evaluated in this study.

2. Materials and Methods

2.1 Design

The principle of the airflow-induced harvester based on a harmonica reed is as follows. Air pressure generated by an airflow bends a cantilever. The deformation of the cantilever opens an air gap between the tip and frame of the device. As the cantilever is bent, the air pressure decreases and the restoring force of the cantilever increases. This process occurs whenever a sufficient airflow is introduced into the device. The air pressure instability, originating from the air gap between the movable structure and a fixed wall, causes the mechanical structure to oscillate, resulting in a resonant vibration. The air pressure instability depends on the structure's stiffness and shape. The motion equation of the ramped model for a resonantly vibrating reed is⁽¹⁸⁾

$$m\ddot{y} + D\dot{y} + ky + \Gamma^2 Z_{cp//RL}\dot{y} = F, \quad (1)$$

where y is the displacement of the reed when an external force $F (=F_o \sin \omega t)$ is applied, m is the equivalent mass, D is the equivalent damping coefficient, k is the equivalent spring constant, Γ is the electrical-mechanical conversion factor (equal to the electrical charge generated per mechanical displacement), and $Z_{cp//RL}$ is the impedance of the output circuit model (piezoelectric capacitor and load resistance connected in parallel). Since the output voltage V_o is

$$V_o = \Gamma Z_{cp//RL} \dot{y}, \quad (2)$$

the output power P_o at the load resistance is

$$P_o = V_o \Gamma \dot{y} = (\Gamma \dot{y})^2 Z_{cp//RL}. \quad (3)$$

Therefore, the output power is proportional to the square of the reed velocity. By solving these equations, the output power and tip displacement can be estimated. However, it is difficult to predict the input force originating from an unstable pressure fluctuation near the cantilever because of the complex fluid–structure interaction.⁽¹⁹⁾ Therefore, the prototype device is fabricated and experimentally characterized.

Similarly to harmonica reeds, the designed device was a simple cantilever with a uniform cross section and no proof masses (Fig. 1). To convert mechanical vibration energy into electrical energy, piezoelectric thin films were laminated on the substrate. The cantilever of the energy harvester was 10 mm long, the same as that of a conventional vibration energy harvester,⁽²⁰⁾ and 3 mm wide to ensure a longitudinally warped shape.⁽²¹⁾ For piezoelectric vibration energy harvesters, the electromechanical coupling factor is proportional to the thickness of the piezoelectric layer.⁽²⁰⁾ Therefore, lead zirconate titanate (PZT) thin films with a thickness of 10 μm , whose microfabrication we previously reported,^(20–23) were adopted as the piezoelectric layer of the airflow energy harvesters. Although the optimal thickness of a Si substrate used in a

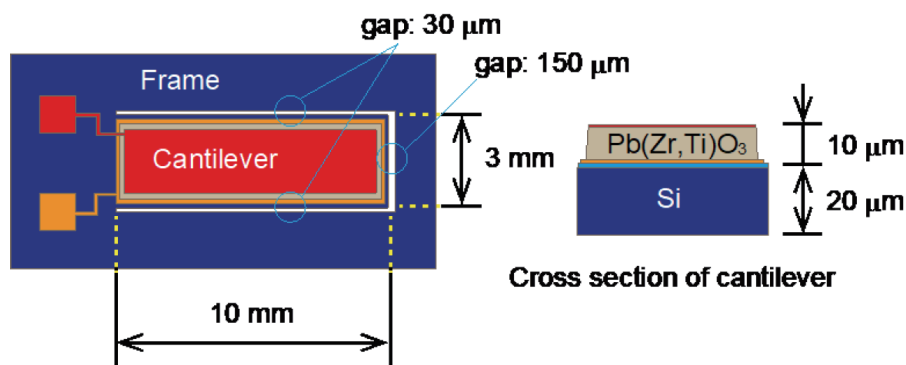


Fig. 1. (Color online) Dimensions of the harvesting device.

conventional vibration energy harvester is $4\ \mu\text{m}$,⁽²⁰⁾ the Si substrate thickness was set to $20\ \mu\text{m}$ because it would have been difficult to control the warpage and the device would have been very fragile if its total thickness was too low. The gaps between the frame and cantilever at the tip and side were 150 and $30\ \mu\text{m}$, respectively. As described in the next section, the cantilever was fabricated with a slightly upward warped shape.

2.2 Fabrication process

The fabrication process is shown in Fig. 2. A silicon-on-insulator wafer with a diameter of $100\ \text{mm}$ and thicknesses of 20 , 1 , and $500\ \mu\text{m}$ for the active, buried oxide, and handle layers, respectively, was thermally oxidized for $280\ \text{min}$ to grow a $1\text{-}\mu\text{m}$ -thick SiO_2 layer on the surface [Fig. 2(a)]. Ti, Pt, SrRuO_3 , and PZT thin films were sequentially sputtered on the wafer using sputtering equipment (CS200-TOKU, ULVAC Inc.), where the $\text{SrRuO}_3/\text{Pt}/\text{Ti}$ layers made up the bottom electrode for the PZT. The thicknesses of Ti, Pt, and SrRuO_3 were 10 , 100 , and $40\ \text{nm}$, respectively, with the Ti used as the adhesion layer between the Pt layer and the substrate, and the Pt layer was the main electrode. The SrRuO_3 , which is electrically conductive, prevented interlayer diffusion between the PZT and the electrode metals. A PZT target with a $\text{Pb}(\text{Zr}_{0.52}\text{Ti}_{0.48})\text{O}_3$ (morphotropic phase boundary) composition containing 15% excess PbO (diameter = $300\ \text{mm}$) was used for sputtering. To obtain a thicker PZT thin film, multistep sputtering was used.⁽²³⁾ The PZT layer was formed by alternating four PZT depositions (layer thickness = $2.5\ \mu\text{m}$) with exposure to air at room temperature, resulting in a $10\text{-}\mu\text{m}$ -thick PZT film with good piezoelectric characteristics. A Au/Cr [$100/20\ \text{nm}$] top electrode was deposited using sputtering equipment (JEC-SP360M, JEOL) [Fig. 2(b)], and the sputtering conditions are

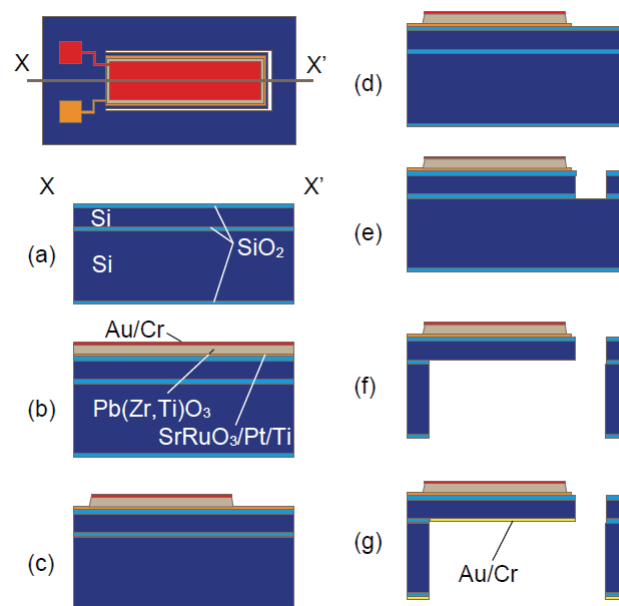


Fig. 2. (Color online) Fabrication process flow.

summarized in Table 1. The Au/Cr was patterned by an iodine-based Au etchant (AURUM 302, Kanto Kagaku) and a Cr etchant (SEK-1, Konan Muki Co. Ltd.) based on a perchloric acid/ceric ammonium nitrate solution. The PZT was dry-etched by a gas mixture plasma of Cl_2 , BCl_3 , and CH_4 , and the top electrode and PZT were sequentially patterned using an identical resist pattern [Fig. 2(c)]. The bottom electrodes were dry-etched using a gas mixture plasma of Cl_2 and Ar [Fig. 2(d)] under the previously reported etching conditions.⁽²⁴⁾ The top SiO_2 , Si, and buried SiO_2 were sequentially dry-etched [Fig. 2(e)], where CHF_3 gas plasma was used to etch the SiO_2 . Deep reactive ion etching was performed on Si using MUC-21 etching equipment (Sumitomo Precision), and the other dry etching processes were conducted using 101iPH etching equipment (SAMCO). After wet etching of the bottom SiO_2 using buffered hydrofluoric acid, the handle layer of Si was etched through. The buried oxide layer underneath the cantilever was sequentially etched by dry etching to reduce the residual strain of the cantilever structure [Fig. 2(f)]. Finally, Cr with a thickness of 120 nm was sputtered on the back side of the cantilever to compensate for the residual tensile stress of the PZT and bottom electrode [Fig. 2(g)]. A photograph of the fabricated device is shown in Fig. 3.

2.3 Poling treatment and stress compensation

When an electric field is applied to the coercive field of a piezoelectric film (poling treatment), randomly distributed domains rotate and align. This poling treatment is essential for obtaining good piezoelectric properties. However, this domain rotation macroscopically

Table 1
Sputtering conditions of the deposited films.

	Material	RF power (W/cm^2)	Temperature ($^{\circ}\text{C}$)	Gas flowrate (sccm)	Pressure (Pa)
Top electrode	Au	1.27	Room temp.	Ar 4	1.0
	Cr	2.54	Room temp.	Ar 1	0.5
Piezoelectric layer	$\text{Pb}(\text{Zr},\text{Ti})\text{O}_3$	1.41	475	Ar/ O_2 39/0.5	0.21
	SrRuO_3	6.37	530	Ar/ O_2 80/20	0.44
Bottom electrode	Pt	6.37	530	Ar 40	0.44
	Ti	6.37	530	Ar 40	0.44
Stress compensation	Cr	2.54	Room temp.	Ar 1	0.5

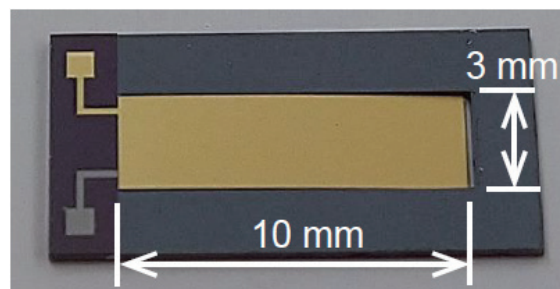


Fig. 3. (Color online) Fabricated harvesting device.

becomes residual stress. Since the initial shape of the airflow harvester can influence the output performance, the position of the cantilever tip is important. The tip position of the fabricated cantilever relative to the frame was $-250\ \mu\text{m}$. For the same structure without Cr deposition, the tip position was $860\ \mu\text{m}$. In this study, a unipolar sinusoidal wave with a peak-to-peak voltage of $70\ \text{V}$ at a frequency of $100\ \text{Hz}$ was applied to the PZT film for $10\ \text{min}$ as poling treatment. The tip position relative to the frame was changed from -250 to $162\ \mu\text{m}$ and from 860 to $1541\ \mu\text{m}$ for the devices with and without the Cr thin film on the back side, respectively. These changes correspond to tensile stress of the PZT in the longitudinal direction of $42\ \text{MPa}$. Owing to the stress compensation of the Cr sputtering, the cantilever had moderately upward warpage similarly to a harmonica reed.

3. Results

3.1 Characterization of PZT film

To confirm the piezoelectricity of the PZT thin film, its dielectric and piezoelectric properties were evaluated. Using an LCR (inductance–capacitance–resistance) meter, we measured the relative permittivity and dielectric tangential loss to be 1240 and 0.03 , respectively. The capacitance C_p of the cantilever was $33\ \text{nF}$. The displacement of the cantilever tip when voltage was applied was measured using a Doppler vibrometer. The frequency profile of the displacement of the cantilever tip under a peak-to-peak voltage of $0.4\ \text{V}$ is shown in Fig. 4. The resonant frequency and quality factor were $241\ \text{Hz}$ and 57 , respectively. The piezoelectric constant d_{31} was estimated under the quasi-static condition at $40\ \text{Hz}$ using the relationship between the applied voltage and the displacement of the cantilever tip. The measured tip displacement and piezoelectric constant are shown in Fig. 5. The piezoelectric constant of around $-70\ \text{pm/V}$ is comparable to that of conventional polycrystalline PZT thin films.^(22,23)

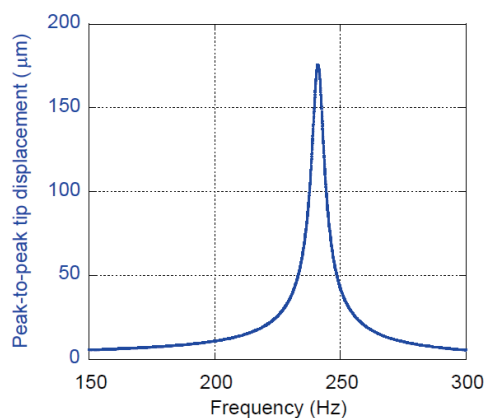


Fig. 4. (Color online) Frequency response of fabricated harvester when a sinusoidal voltage was applied (peak-to-peak voltage of $0.4\ \text{V}$).

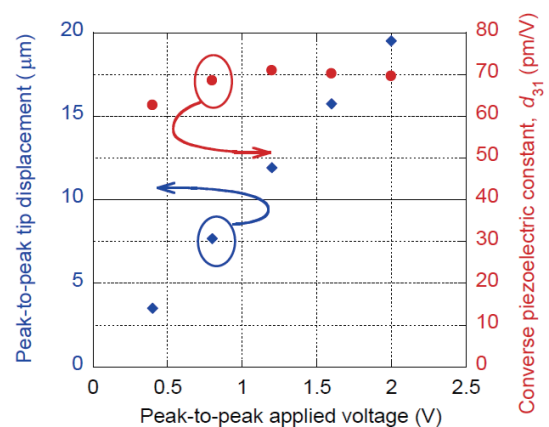


Fig. 5. (Color online) Tip displacement versus applied voltage under quasi-static conditions ($40\ \text{Hz}$).

3.2 Energy harvesting from airflow

The experimental setup for power generation from an airflow is depicted in Fig. 6. An airflow generated by a fan passed through a duct with inner dimensions of $20 \times 20 \times 60 \text{ cm}^3$ length to a metal net where the device was fixed. The flowrate at the device was measured using an anemometer. The top and bottom electrodes were connected to a load resistor and oscilloscope in parallel, and the output power was calculated from the measured voltage and resistance. The vibration frequency of the harvester became resonant due to airflow-induced self-excitation. The optimum load resistance was estimated to be $20.1 \text{ k}\Omega$ from the resonant frequency and capacitance of the PZT ($= 1/\omega_0 C_{pzt}$).^(18,20) The relationship between the output power and load resistance was then measured at a flow velocity of 3.3 m/s to obtain the optimum load resistance (Fig. 7). A peak output power of $3.5 \text{ }\mu\text{W}$ was obtained at a load resistance of $22 \text{ k}\Omega$, in good agreement with the estimation. The flowrate dependence of the output power was measured under the load resistance of $22 \text{ k}\Omega$ (Fig. 8). Even when the flow velocity was very low, the harvesting device oscillated resonantly. The cut-in flowrate was 1.2 m/s . The power density per unit device area, including the Si frame, was $3.97 \text{ }\mu\text{W}/\text{cm}^2$, which is sufficient to power several

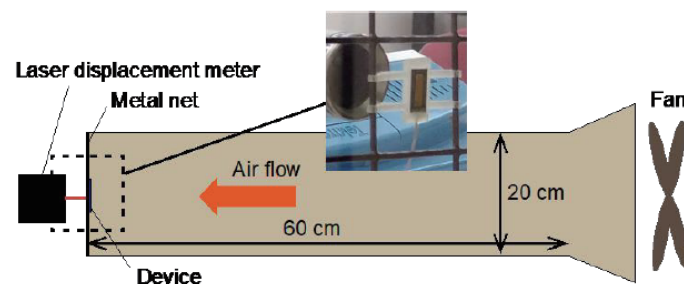


Fig. 6. (Color online) Experimental setup for energy harvesting from airflow.

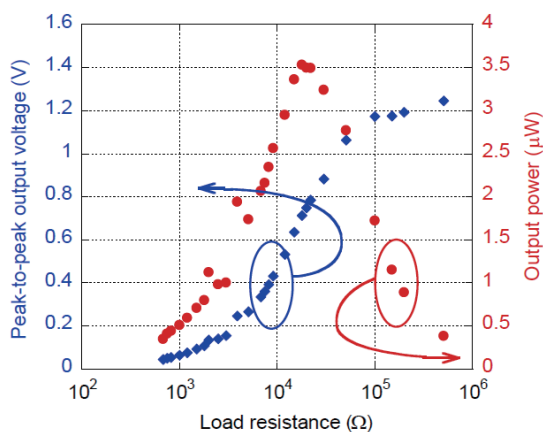


Fig. 7. (Color online) Load resistance dependences of output voltage and power at flowrate of 3.3 m/s .

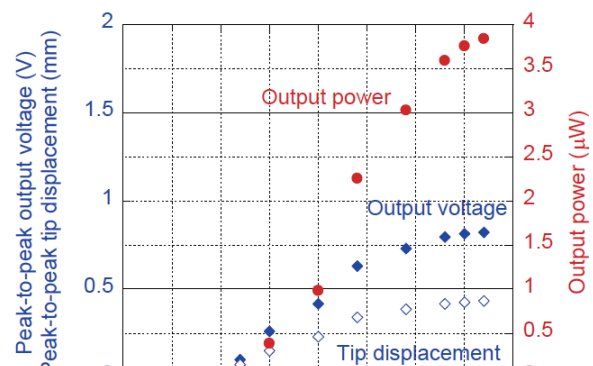


Fig. 8. (Color online) Flow velocity dependence of output power.

Table 2
Comparison of devices for harvesting energy from airflow.

Ref No.	Type	Output power (μW)	Flow velocity (m/s)	Cut-in flow velocity (m/s)	Size (mm) $L \times W \times t$	Power density ($\mu\text{W}/\text{mm}^3$)
9	Bulk	880	12.9	6.45	$58 \times 16 \times 0.3$	3.16
10	Bulk	4000	9	2.8	$200 \times 15 \times 0.8$	1.67
11	Bulk	6300	12	9	$100 \times 20 \times 0.2$	15.75
12	MEMS	0.0033	15.6	3.9	$3 \times 0.3 \times 0.008$	0.458
13	MEMS	0.0387	15.6	3.2	$3.3 \times 2 \times 0.4$	0.015
14	MEMS	2.27	16.3	13.1	$10 \times 8 \times 0.51$	0.9
This work	MEMS	3.84	3.7	1.2	$10 \times 3 \times 0.03$	4.27

sensors and peripheral circuits. These results are for the harvester with a Cr thin film on the back side of the cantilever. For the devices without the Cr film, self-excited oscillation did not occur below a flow velocity of 3.9 m/s. Larger warpage can increase the cut-in velocity. In addition, devices that were mounted upside down in the experimental setup did not vibrate. These results indicate that the warpage of the cantilever should be controlled to enable power generation at a low flow velocity.

4. Discussion

A comparison of the performances of energy harvesters based on harmonica reeds is given in Table 2, in which the sizes do not include the resonant cavities and frames. The bulk harvesters can generate a large output power. These devices can replace small wind turbines in a large wind velocity range. However, these bulk harvesters require a high flow velocity for power generation. A high flow velocity is also required for conventional MEMS harvesters. The conventional MEMS harvesters in Refs. 12 and 13 employ a proof mass to generate power not only from an airflow but also from excitation due to acceleration. The proof mass may reduce the stability of the air pressure near the device. The instability of the pressure near the sensitive gap region between the frame and tip can affect the cut-in flow velocity. A rigid proof mass located on the cantilever tip can increase the cut-in flow velocity. The harvester in Ref. 14 had no frame but was located parallel to the airflow. This device was almost a VIV-type harvester. The intentionally fabricated warped shape and the gap between the device and the frame in this study reduced the cut-in flow velocity. Even at a very low flow velocity, a relatively large output power was obtained with the proposed device, which was attributed to the thick PZT thin film. The effect of the in-plane gap and out-of-plane opening between the cantilever tip and the frame should be investigated to enable a comparison of devices with different flow velocity sensitivities and to further improve the device performance. Moreover, analysis of the fluid–structure coupling near the cantilever can enable precise prediction of the device performance.

5. Conclusions

We designed a novel airflow-induced MEMS energy-harvesting device based on the principle of a harmonica reed with the aim of reducing the cut-in flow velocity. The cut-in flow velocity

was reduced by controlling the upward warpage of the PZT/Si cantilever of the device by sputtering a Cr thin film on the back side of the cantilever. After poling treatment, the position of the cantilever tip relative to the frame was 162 μm . This controlled warpage reduced the cut-in velocity of the harvesting device to 1.2 m/s, which is the lowest value reported to the authors' knowledge. The thick PZT film in the device, deposited by multistep sputtering, generated a relatively large output power of 3.84 μW from an airflow with a low velocity of 3.7 m/s.

Acknowledgments

This research was partially supported by the Japan Society for the Promotion of Science (JSPS) Grant-in-Aid for Scientific Research (B) 20H02120 and Japan Science and Technology Agency (JST) CREST Grant Number JPMJCR20Q2, Japan.

References

- 1 S. P. Beeby, M. J. Tudor, and N. M. White: *Meas. Sci. Tech.* **17** (2006) R175. <https://doi.org/10.1088/0957-0233/17/12/R01>
- 2 S. Roundy, P. K. Wright, and J. Rabaey: *Comput. Commun.* **26** (2003) 1131. [https://doi.org/10.1016/S0140-3664\(02\)00248-7](https://doi.org/10.1016/S0140-3664(02)00248-7)
- 3 P. D. Mitcheson, T. C. Green, E. M. Yeatman, and A. S. Holmes: *J. Microelectromech. Syst.* **13** (2004) 429. <https://doi.org/10.1109/JMEMS.2004.830151>
- 4 S. Aphayvong, T. Yoshimura, S. Murakami, K. Kanda, and N. Fujimura: *Jpn. J. Appl. Phys.* **59** (2020) SPPD04. <https://doi.org/10.35848/1347-4065/abad16>
- 5 P. Pillatsch, E. M. Yeatman, and A. S. Holmes: *Smart Mater. Struct.* **21** (2012) 115018. <https://doi.org/10.1088/0964-1726/21/11/115018>
- 6 W. Liu, F. Formosa, A. Badel, Y. Wu, and A. Agbossou: *Sens. Actuators, A* **216** (2014) 105. <https://doi.org/10.1016/j.sna.2014.04.040>
- 7 M. Aramaki, T. Yoshimura, S. Murakami, K. Kanda, and N. Fujimura: *Appl. Phys. Lett.* **114** (2019) 133902. <https://doi.org/10.1063/1.5093956>
- 8 Q. Wen, X. He, Z. Lu, R. Streiter, and T. Otto: *Nano Mater. Sci.* **3** (2021) 170. <https://doi.org/10.1016/j.nanoms.2021.04.001>
- 9 D. St. Clair, A. Bibo, V. R. Sennakesavababu, M. F. Daqaq, and G. Li: *Appl. Phys. Lett.* **96** (2010) 144103. <https://doi.org/10.1063/1.3385780>
- 10 J. Ji, F. Kong, L. He, Q. Guan, and Z. Feng: *Jpn. J. Appl. Phys.* **49** (2010) 050204. <https://doi.org/10.1143/JJAP.49.050204>
- 11 Y. Zhang, C. Pan, X. Meng, and L. Yu: *Proc. 2015 IEEE Symposium on Piezoelectricity, Acoustic waves, and Device Applications, (IEEE 2015)* 219–222. <https://doi.org/10.1109/SPAWDA.2015.7364476>
- 12 H. Liu, S. Zhang, R. Kathuresan, T. Kobayashi, and C. Lee: *Appl. Phys. Lett.* **100** (2012) 223905. <https://doi.org/10.1063/1.4723846>
- 13 H. Liu, S. Zhang, T. Kobayashi, T. Chen, and C. Lee: *Micro & Nano Lett.* **9** (2014) 286. <https://doi.org/10.1049/mnl.2013.0750>
- 14 X. He, Z. Shang, Y. Cheng, and Y. Zhu: *J. Micromech. Microeng.* **23** (2013) 125009. <https://iopscience.iop.org/article/10.1088/0960-1317/23/12/125009>
- 15 M. Y. Zalaria, M. Y. Al-Halk, and M. J. Haji: *Appl. Phys. Lett.* **107** (2015) 023901. <https://doi.org/10.1063/1.4926876>
- 16 S. Li, J. Yuan, and H. Lipson: *J. Appl. Phys.* **109** (2011) 026104. <https://doi.org/10.1063/1.3525045>
- 17 L. Milot and C. Baumann: *Acta Acustica United with Acustica* **93** (2007) 122.
- 18 M. Renaud, K. Karakaya, T. Sterken, P. Fiorini, C. Van Hoof, and R. Puers: *Sens. Actuators, A* **145–146** (2008) 380. <https://doi.org/10.1016/j.sna.2007.11.005>
- 19 Y. Tsujiura, E. Suwa, T. Nishi, F. Kurokawa, H. Hida, and I. Kanno: *Sens. Actuators, A* **261** (2017) 295. <https://doi.org/10.1016/j.sna.2017.04.031>
- 20 K. Kanda, S. Hirai, T. Fujita, and K. Maenaka: *Sens. Actuators, A* **281** (2018) 299. <https://doi.org/10.1016/j.sna.2018.09.018>

- 21 S. Hirai, K. Kanda, T. Fujita, and K. Maenaka: *Jpn. J. Appl. Phys.* **58** (2019) SLLD07. <https://doi.org/10.7567/1347-4065/ab362f>
- 22 R. Sano, J-I. Inoue, K. Kanda, T. Fujita, and K. Maenaka: *Jpn. J. Appl. Phys.* **54** (2015) 10ND03. <https://doi.org/10.7567/JJAP.54.10ND03>
- 23 K. Kanda, T. Koyama, T. Yoshimura, S. Murakami, and K. Maenaka: *IEEE Trans. Ultrason. Ferroelectr. Freq. Control* **68** (2021) 1988. <https://doi.org/10.1109/TUFFC.2020.3039230>
- 24 K. Kanda, Y. Iga, J. Matsuoka, T. Fujita, K. Higuchi, and K. Maenaka: *IEEJ Trans. SM.* **130** (2010) 124 (in Japanese). <https://doi.org/10.1541/ieejsmas.130.124>